

March 9, 2021

AN ACTIVE CURVE APPROACH FOR TOMOGRAPHIC RECONSTRUCTION OF BINARY RADIALLY SYMMETRIC OBJECTS

I. ABRAHAM¹, R. ABRAHAM AND M. BERGOUNIOUX²

Abstract. This paper deals with a method of tomographic reconstruction of radially symmetric objects from a single radiograph, in order to study the behavior of shocked material. The usual tomographic reconstruction algorithms such as generalized inverse or filtered back-projection cannot be applied here because data are very noisy and the inverse problem associated to single view tomographic reconstruction is highly unstable. In order to improve the reconstruction, we propose here to add some a priori assumptions on the looked after object. One of these assumptions is that the object is binary and consequently, the object may be described by the curves that separate the two materials. We present a model that lives in BV space and leads to a non local Hamilton-Jacobi equation, via a level set strategy. Numerical experiments are performed (using level sets methods) on synthetic objects.

1991 Mathematics Subject Classification. 68U10, 44A12, 49N45.

The dates will be set by the publisher.

1. INTRODUCTION

Medical scanner is the most used application of tomographic reconstruction. It allows to explore the interior of a human body. In the same way, industrial tomography explores the interior of an object and is often used for non-destructive testing.

We are interested here in a very specific application of tomographic reconstruction for a physical experiment described later. The goal of this experiment is to study the behavior of a material under a shock. We obtain during the deformation of the object an X-ray radiography by high speed image capture. We suppose this object is radially symmetric, so that one radiograph is enough to reconstruct the 3D object.

Keywords and phrases: Tomography, Optimization, Segmentation, Level set.

¹ CEA Ile de France- BP 12

91680 Bruyères le Châtel

FRANCE

isabelle.abraham@cea.fr

² Laboratoire MAPMO- Fédération Denis Poisson

Université d'Orléans

BP 6759

ORLEANS cedex 02

FRANCE

romain.abraham@univ-orleans.fr, maitine.bergounioux@univ-orleans.fr

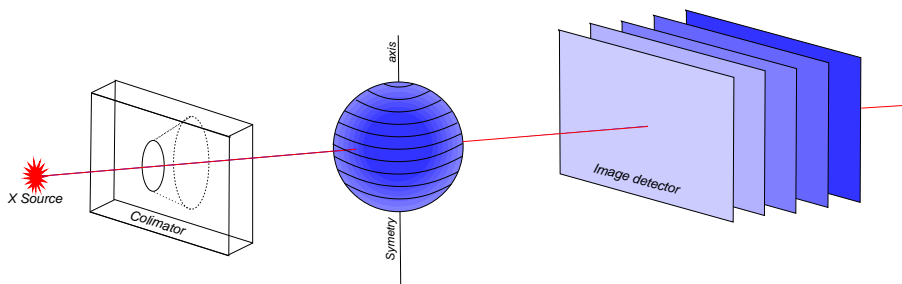


FIGURE 1. Experimental setup

Several authors have proposed techniques (standard in medical tomography) for tomographic reconstruction when enough projections (from different points of view) are available: this allows to get an analytic formula for the solution (see for instance [9] or [6]). These methods cannot be used directly when only a few number of projections is known. Some alternative methods have been proposed in order to partially reconstruct the densities (see for instance [5]). We are interesting here in single view tomographic reconstruction for radially symmetric object (see for instance [8] for a more complete presentation of the subject). As any tomographic reconstruction, this problem leads to an ill-posed inverse problem. As we only have one radiograph, data are not very redundant and the ill-posed character is even more accurate.

We present here a tomographic method adapted to this specific problem, originally developed in [1], and based on a curve evolution approach. The main idea is to add some a priori knowledge on the object we are studying in order to improve the reconstruction. The object may then be described by a small set of characters (in this case, they will be curves) which are estimated by the minimization of an energy functional. This work is very close to another work by Feng and al [7]. The main difference is the purpose of the work: whereas they are seeking recovering textures, we are looking for accurate edges. It is also close to the results of Bruandet and al [3]. However, the present work handles very noisy data and highly unstable inverse problems, and shows how this method is powerful despite these perturbations. Further, we take here into account the effects of blur (which may be non-linear) and try to deconvolve the image during the reconstruction.

Let us mention at this point that our framework is completely different from the usual tomographic point of view, and usual techniques (such as filtered back-projection) are not adapted to our case. Indeed, usually, as the X-rays are supposed to be parallel (this is also the case here), the “horizontal” slices of the object are supposed to be independent and studied separately. Usual regularization techniques deal with one slice and regularize this particular slice. Here, because of the radial symmetry, the slices are composed of concentric annulus and do not need any regularization. The goal of this work is to add some consistency between the slices in order to improve the reconstruction.

The paper is organized as follows. First we present the physical experiment whose data are extracted and explain what are the motivations of the work. Next, we introduce the projection operator. In Section 4, we present a continuous model with the suitable functional framework and prove existence result. Section 5 is devoted to formal computation of the energy derivative in order to state some optimality conditions. In Section 6, a front propagation point of view is adopted and

the level set method leads to a non local Hamilton-Jacobi equation. In the last section, we present some numerical results and give hints for numerical schemes improvement.

2. EXPERIMENT

This work is part of some physical experiments whose goal is the study of the behavior of shocked material. The present experiment consists in making a hull of well known material implode using surrounding explosives. The whole initial physical setup (the hull, the explosives ...) are radially symmetric. A reasonable assumption is to suppose that during the implosion, everything remains radially symmetric.

Physicists are looking for the shape of the interior at some fixed time of interest. At that time, the interior may be composed of several holes which also may be very irregular. Figure 3 is a synthetic object that contains all the standard difficulties that may appear. These difficulties are characterized by:

- Several disconnected holes.
- A small hole located on the symmetry axis (which is the area where the details are difficult to recover).
- Smaller and smaller details on the boundary of the top hole in order to determine a lower bound detection.

To achieve this goal, a X-rays radiograph is obtained. In order to extract the desired informations, a tomographic reconstruction must be performed. Let us note here that, as the object is radially symmetric, a single radiography is enough to compute the reconstruction.

A radiography measures the attenuation of X-rays through the object. A point on the radiography will be determined by its coordinates (u, v) in a Cartesian coordinates system where the v -axis will be the projection of the symmetry axis. If I_0 is the intensity of the incident X-rays flux, the measured flux I at a point (u, v) is given by

$$I = I_0 e^{-\int \mu(r, \theta, z) dl}$$

where the integral operates along the ray that reaches the point (u, v) of the detector, dl is the infinitesimal element of length along the ray and μ is the local attenuation coefficient. For simplicity, we will consider that this coefficient is proportional to the material density. To deal with linear operators, we take the Neperian logarithm of this attenuation and will call the transformation

$$\rho \longmapsto \int \rho dl$$

the projection operator.

Through the rest of the paper, in order to simplify the expression of the projection operator, we will suppose that the X-ray source is far enough away from the object so that we may consider that the rays are parallel, and orthogonal to the symmetry axis. As a consequence, the horizontal slices of the object may be considered separately to perform the projection.

As the studied object is radially symmetric, we will work in a system of cylinder coordinates (r, θ, z) where the z -axis is the symmetry axis. The object is then described by the density at the

point (r, θ, z) , which is given by a function f which depends only on (r, z) by symmetry. In the text, the notation f will always refer to the density of the object. A typical function f is given in Figure 2. It represents an object composed of concentric shells of homogeneous materials (called the “exterior” in what follows) surrounding a ball (called the “interior”) of another homogeneous material that contains some empty holes. This figure may be viewed as a slice of the object by a plane that contains the symmetry axis. To recover the 3D-object, it suffices to perform a rotation of this image around the z axis. For instance, the two round white holes in the center are in fact the slice of a torus. As the looked-after characteristic of the object is the shape of the holes, we will focus only on the interior of the object (see Figure 3). We here handle only binary objects composed of one homogeneous material (in black) and some holes (in white).



FIGURE 2. Slice of a typical binary radially symmetric object by a plane that contains the symmetry axis (the z -axis).



FIGURE 3. Zoom on the interior of the object of Figure 2. The homogeneous material is in black whereas the holes are in white.

3. A VARIATIONAL APPROACH

3.1. The projection operator

We first explicit the projection operator and its adjoint.

Proposition 3.1. *In the case of a radially symmetric object, the projection operator, denoted by H , is given, for every function $f \in L^\infty(\mathbb{R}_+ \times \mathbb{R})$ with compact support, by*

$$\forall (u, v) \in \mathbb{R} \times \mathbb{R} \quad Hf(u, v) = 2 \int_{|u|}^{+\infty} f(r, v) \frac{r}{\sqrt{r^2 - u^2}} dr. \quad (3.1)$$

Proof - Consider a 3D-object which is described by a function $\tilde{f}(x, y, z)$ (Cartesian coordinates system). The projection operator H is

$$H\tilde{f}(u, v) = \int_{\mathbb{R}} \tilde{f}(x, u, v) dx .$$

In the case of radially symmetric object, we parametrize the object by a function $f(r, z)$ with cylinder coordinates. Therefore

$$\tilde{f}(x, y, z) = f(\sqrt{x^2 + y^2}, z) .$$

Then, we have, for $u \geq 0$

$$Hf(u, v) = \int_{\mathbb{R}} \tilde{f}(x, u, v) dx = \int_{\mathbb{R}} f(\sqrt{x^2 + u^2}, v) dx = 2 \int_0^{+\infty} f(\sqrt{x^2 + u^2}, v) dx .$$

We perform the following change of variable

$$r = \sqrt{x^2 + u^2}, \quad x \geq 0 \iff x = \sqrt{r^2 - u^2}, \quad r \geq u ,$$

to get

$$Hf(u, v) = 2 \int_u^{+\infty} f(r, v) \frac{r}{\sqrt{r^2 - u^2}} dr .$$

For $u < 0$, we have

$$Hf(u, v) = 2 \int_{-\infty}^u f(r, v) \frac{|r|}{\sqrt{r^2 - u^2}} dr .$$

Using the change of variable $u : to -u$ and the fact that $r \mapsto f(r, v)$ is even, by symmetry, we get

$$Hf(u, v) = 2 \int_{|u|}^{+\infty} f(r, v) \frac{r}{\sqrt{r^2 - u^2}} dr.$$

□

Remark 3.1. Operator H may be defined by density on measurable functions f such that all the partial applications $f(\cdot, z)$ belong to $L^2(\mathbb{R}_+)$. Then, all the functions $Hf(\cdot, v)$ belong to the space $BMO(\mathbb{R})$ of bounded mean oscillations functions :

$$BMO(\mathbb{R}) = \left\{ f : \mathbb{R} \rightarrow \mathbb{R} \mid \sup_{R>0} \left(\frac{1}{R} \int_{|x-y|<R} |f(x) - f_R(y)| dx \right) < +\infty \right\},$$

where $f_R(y) = \frac{1}{2R} \int_{y-R}^{y+R} f(x) dx$. For more details, one can refer to [13].

In the sequel, we will need to handle functions f that are defined on \mathbb{R}^2 (instead of on $\mathbb{R}_+ \times \mathbb{R}$). We thus define the operator H for function $f \in L^\infty(\mathbb{R}^2)$ with compact support by

$$Hf(u, v) = 2 \int_{|u|}^{+\infty} f(\operatorname{sgn}(u)r, v) \frac{r}{\sqrt{r^2 - u^2}} dr$$

although this has no more physical meaning. Here, the function sgn is defined by

$$\operatorname{sgn}(x) = \begin{cases} 1 & \text{if } x \geq 0, \\ -1 & \text{if } x < 0. \end{cases}$$

We shall also need the back-projection that is the adjoint operator H^* of H ; it can be computed in a similar way.

Proposition 3.2. The adjoint operator (in L^2) H^* of the projection operator is given, for every function $g \in L^\infty(\mathbb{R}^2)$ with compact support by :

$$\forall r \in \mathbb{R}, \forall z \in \mathbb{R}, \quad H^*g(r, z) = 2 \int_0^{|r|} g(\operatorname{sgn}(r)u, z) \frac{|r|}{\sqrt{r^2 - u^2}} du. \quad (3.2)$$

Proof - The adjoint operator H^* of H is the unique operator such that, for every f and g in $L^\infty(\mathbb{R}^2)$ with compact support,

$$\int_{-\infty}^{+\infty} \int_{-\infty}^{+\infty} Hf(u, v) g(u, v) dv du = \int_{-\infty}^{+\infty} \int_{-\infty}^{+\infty} f(r, z) H^*g(r, z) dr dz .$$

Using (3.1) and Fubini's theorem, we get

$$\begin{aligned}
& \int_{-\infty}^{+\infty} \int_{-\infty}^{+\infty} Hf(u, v) g(u, v) dv du \\
&= 2 \int_{u=-\infty}^{u=0} \int_{v=-\infty}^{v=+\infty} \int_{r=|u|}^{r=+\infty} f(-r, v) \frac{r}{\sqrt{r^2 - u^2}} g(u, v) dv du dr \\
&\quad + 2 \int_{u=0}^{u=+\infty} \int_{v=-\infty}^{v=+\infty} \int_{r=u}^{r=+\infty} f(r, v) \frac{r}{\sqrt{r^2 - u^2}} g(u, v) dv du dr \\
&= 2 \int_{v=-\infty}^{v=+\infty} \int_{r=0}^{r=+\infty} \int_{u=-r}^{u=0} \frac{r}{\sqrt{r^2 - u^2}} f(-r, v) g(u, v) du dr dv \\
&\quad + 2 \int_{v=-\infty}^{v=+\infty} \int_{r=0}^{r=+\infty} \int_{u=0}^{u=r} \frac{r}{\sqrt{r^2 - u^2}} f(r, v) g(u, v) du dr dv \\
&= 2 \int_{v=-\infty}^{v=+\infty} \int_{r=0}^{r=+\infty} \int_{u=r}^{u=0} \frac{-r}{\sqrt{r^2 - u^2}} f(r, v) g(u, v) du (-dr) dv \\
&\quad + 2 \int_{v=-\infty}^{v=+\infty} \int_{r=0}^{r=+\infty} \int_{u=0}^{u=r} \frac{r}{\sqrt{r^2 - u^2}} f(r, v) g(u, v) du dr dv \\
&= 2 \int_{v=-\infty}^{v=+\infty} \int_{r=-\infty}^{r=+\infty} \int_{u=0}^{u=r} \frac{r}{\sqrt{r^2 - u^2}} f(r, v) g(u, v) du dr dv \\
&= 2 \int_{v=-\infty}^{v=+\infty} \int_{r=-\infty}^{r=+\infty} \int_{u=0}^{u=|r|} \frac{|r|}{\sqrt{r^2 - u^2}} f(r, v) g(\text{sgn}(r)u, v) du dr dv
\end{aligned}$$

So we obtain the following expression for the back projection :

$$H^* g(r, z) = 2 \int_0^{|r|} \frac{|r|}{\sqrt{r^2 - u^2}} g(\text{sgn}(r)u, z) du .$$

□

3.2. Toward a continuous model

Thanks to the symmetry, this operator characterizes the Radon transform of the object and so is invertible; one radiograph is enough to reconstruct the object. The inverse operator is given, for an almost everywhere differentiable function g with compact support, and for every $r > 0$, by

$$H^{-1}g(r, z) = -\frac{1}{\pi} \int_r^{+\infty} \frac{\partial}{\partial x} g(x, z) \frac{dx}{\sqrt{x^2 - r^2}} .$$

Because of the derivative term, the operator H^{-1} is not continuous. Consequently, a small variation on the measure g leads to significant errors on the reconstruction. As our radiographs are strongly perturbed, applying H^{-1} to our data leads to a poor reconstruction. Due to the experimental setup they are also two main perturbations:

- A blur, due to the detector response and the X-ray source spot size.

- A noise.

Others perturbations such as scattered field, motion blur... also exist but are neglected in this study. We denote by F the effect of blurs. We will consider the following simplified case where F is supposed to be linear

$$F(k) = N * k \quad (3.3)$$

where $*$ is the usual convolution operation, k is the projected image and N is a positive symmetric kernel.

Remark 3.2. *A more realistic case stands when the convolution operates on the intensity : then F is of the form*

$$F(k) = \frac{-1}{\nu} \ln \left(e^{-\nu k} * N \right)$$

where ν is the multiplicative coefficient between the density and the attenuation coefficient. Some specific experiments have been carried out to measure the blur effect. Consequently, we will suppose that, in both cases, the kernel N is known. The linear blur is not realistic but is treated here to make the computations simpler for the presentation.

The noise is supposed for simplicity to be an additive Gaussian white noise of mean 0, denoted by ε . Consequently, the projection of the object f will be

$$g = F(Hf) + \varepsilon.$$

The comparison between the theoretical projection $F(Hf)$ and the perturbed one is shown on Figure 4. The reconstruction using the inverse operator H^{-1} applied to g is given by Figure 5. The purpose of the experiment is to separate the material from the empty holes and consequently to precisely determine the frontier between the two areas, which is difficult to perform on the reconstruction of Figure 5.

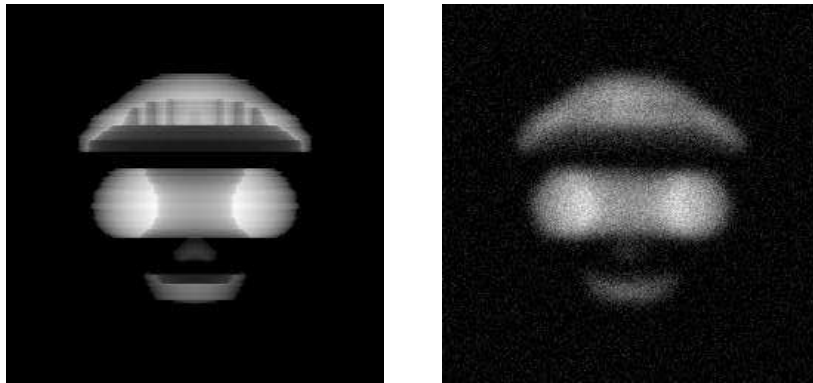


FIGURE 4. Left-hand side: theoretical projection $F(Hf)$ of the object of Figure 3. Right-hand side: real projection of the same object with realistic noise and blur.

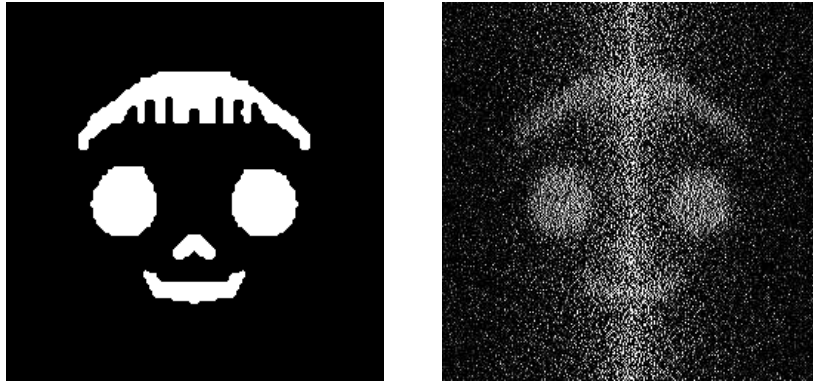


FIGURE 5. Comparison between the real object on the left-hand side and the reconstruction computed with H^{-1} applied to the real projection on the right-hand side.

It is clear from Figure 5 that the use of the inverse operator is not suitable. In order to improve the reconstruction, we must add some a priori knowledge on the object to be reconstructed. Indeed the object that we reconstruct must satisfy some physical property.

We chose to stress on two points:

- The center of the object is composed of one homogeneous known material's density with some holes inside.
- There cannot be any material inside a hole.

In a previous work [10], J.M. Lagrange reconstructed the exterior of the object. In this reconstruction, the density of the material at the center of the object is known, only the holes are not reconstructed. In other words, we can reconstruct an object without holes and we can compute (as H and F are known) the theoretical projection of this reconstruction. We then act as if the blurred projection was linear and subtract the projection of the non-holed object to the data. In what follows, we will call experimental data this subtracted image which corresponds to the blurred projection of a “fictive” object of density 0 with some holes of known “density” $\lambda > 0$. Consequently, the space of admitted objects will be the set of functions f that take values in $\{0, \lambda\}$. This space of functions will be denoted \mathcal{F} in the sequel.

The second hypothesis is more difficult to take into account. We chose in this work to tackle the problem via an energy minimization method where the energy functional is composed of two terms: the first one is a matching term, the second one is a penalization term which tries to handle the second assumption. The matching term will be a L^2 -norm which is justified by the Gaussian white noise.

Remark 3.3. *In the case where F is not linear, the exact method to remove the exterior is to operate the blur function on the addition of the known exterior and the center. For the sake of simplicity, we will not use this method and will consider that the errors are negligible when subtracting the projections.*

Let us first describe more precisely the set \mathcal{F} . This time, the functions $f \in \mathcal{F}$ will be defined on \mathbb{R}^2 , with values still in $\{0, \lambda\}$, with compact support. Therefore, such a function f will be

characterized by the knowledge of the curves that limit the two areas where f is equal to λ and to 0. Indeed, as the support of the function f is bounded, these curves are disjoint Jordan curves and the density of the inside is λ whereas the density of the outside is 0. Consequently, the energy that we will consider will be a function of γ_f where γ_f is a set of disjoint Jordan curves. For mathematical reasons, we must add an extra-assumption : the curves γ_f are \mathcal{C}^1 so that the normal vector of the curves is well-defined (as an orthogonal vector to the tangent one).

In this continuous framework, the matching term is just the usual L^2 -norm between Hf and the data g (where H is given by (3.1)). So, the first term is

$$E_1(\gamma_f) = \|F(Hf) - g\|_2^2.$$

For the penalization term, we choose

$$E_2(\gamma_f) = \ell(\gamma_f)$$

where $\ell(\gamma_f)$ denotes the length of the curves γ_f . Let us remark that this penalization term may be also viewed as the total variation (up to a multiplicative constant) of the function f because of the binarity. Eventually, the total energy functional is

$$E(\gamma_f) = \|F(Hf) - g\|_2^2 + \alpha \ell(\gamma_f) \quad (3.4)$$

which is an adaptation of the well-known Mumford-Shah energy functional introduced in [11]. The ‘‘optimal’’ value of α may depend on the data.

3.3. A continuous model in BV space

The previous analysis gives the mains ideas for the modelization. Now, we make it precise using an appropriate functional framework. Let Ω be a bounded open subset \mathbb{R}^2 with Lipschitz boundary. We shall consider bounded variation functions. Recall that the space of such functions is

$$BV(\Omega) = \{u \in L^1(\Omega) \mid J(u) < +\infty\}$$

where

$$J(u) = \sup \left\{ \int_{\Omega} u(x) \operatorname{div} \xi(x) dx \mid \xi \in \mathcal{C}_c^1(\Omega), \|\xi\|_{\infty} \leq 1 \right\}, \quad (3.5)$$

where $\mathcal{C}_c^1(\Omega)$ denotes the space of \mathcal{C}^1 functions with compact support in Ω . The space $BV(\Omega)$ endowed with the norm

$$\|u\|_{BV(\Omega)} = \|u\|_{L^1} + J(u),$$

is a Banach space.

If $u \in BV(\Omega)$ its derivative in $\mathcal{D}'(\Omega)$ (distributions) is a bounded Radon measure denoted Du and $J(u)$ is the total variation of $|Du|$ on Ω . Let us recall useful properties of BV-functions ([2]):

Proposition 3.3. *Let Ω be an open subset \mathbb{R}^2 with Lipschitz boundary.*

1. *If $u \in BV(\Omega)$, we get the following decomposition for Du :*

$$Du = \nabla u dx + D^s u,$$

where $\nabla u dx$ is the absolutely continuous part of Du with respect of the Lebesgue measure and $D^s u$ is the singular part.

2. The map $u \mapsto J(u)$ from $BV(\Omega)$ to \mathbb{R}^+ is lower semi-continuous (lsc) for the $L^1(\Omega)$ topology.
3. $BV(\Omega) \subset L^2(\Omega)$ with compact embedding.
4. $BV(\Omega) \subset L^1(\Omega)$ with compact embedding.

We precise hereafter an important continuity property of the projection operator H .

Proposition 3.4. *The projection operator H is continuous from $L^{2+s}(\Omega)$ to $L^p(\Omega)$ for every $p \in [1, +\infty]$ and $s > 0$.*

Proof - It is a direct consequence of Hölder inequality. Let be $s > 0$ and $f \in L^{2+s}(\Omega)$. Its support is included in $\bar{\Omega}$ which is included in some $[-M, +M] \times [-M, +M]$ where $M > 0$ and only depends on Ω . It is clear that Hf is defined everywhere on Ω and, for every $u \geq 0$

$$\begin{aligned} |Hf(u, v)| &= 2 \left| \int_u^{+\infty} f(r, v) \frac{r}{\sqrt{r^2 - u^2}} dr \right| = 2 \left| \int_u^M f(r, v) \frac{r}{\sqrt{r^2 - u^2}} dr \right| \\ &\leq 2 \left[\int_u^M |f(r, v)|^{2+s} dr \right]^{\frac{1}{2+s}} \left[\int_u^M \frac{r^q}{(r+u)^{\frac{q}{2}}} \frac{1}{(r-u)^{\frac{q}{2}}} dr \right]^{\frac{1}{q}} \end{aligned}$$

where $q = 1 + \frac{1}{1+s}$. Therefore

$$|Hf(u, v)| \leq 2 \|f\|_{L^{2+s}} \left[\int_u^M \frac{r^q}{r^{\frac{q}{2}}(r-u)^{\frac{q}{2}}} dr \right] \leq 2 M^{\frac{q}{2}} \|f\|_{L^{2+s}} \left[\int_u^M (r-u)^{-\frac{q}{2}} dr \right]$$

The computations in the case $u < 0$ are similare and lead to the same inequality (with some additional absolute values). As

$$1 - \frac{q}{2} = \frac{s}{2(1+s)} > 0,$$

we get

$$|Hf(u, v)| \leq 2 M^{\frac{q}{2}} \|f\|_{L^{2+s}} \frac{2(1+s)}{s} [M-u]^{\frac{s}{2(1+s)}} \leq C(\Omega, s) \|f\|_{L^{2+s}}; \quad (3.6)$$

here and in the sequel $C(\Omega, s)$ denotes a generic constant depending on s and Ω . So

$$\|Hf\|_{\infty} \leq C(\Omega, s) \|f\|_{L^{2+s}}.$$

As Ω is bounded, this yields

$$\forall f \in L^{2+s}(\Omega), \forall p \in [1, +\infty] \quad \|Hf\|_{L^p(\Omega)} \leq C(\Omega, s) \|f\|_{L^{2+s}}. \quad (3.7)$$

□

As we consider the length of curves, the most suitable functional space to set a variational formulation of the reconstruction problem is $BV(\Omega)$. Therefore, we consider the following minimization problem

$$(\mathcal{P}) \quad \begin{cases} \min \|FHf - g\|_2^2 + \alpha J(f) \\ f \in BV(\Omega) \\ |f(x)| = 1 \text{ a.e. on } \Omega \end{cases}$$

Here

- $\|\cdot\|_2$ stands for the $L^2(\Omega)$ - norm, $g \in L^2(\Omega)$ and $\alpha > 0$.
- The operator F is given by (3.3). Without loss of generality, we may assume (for simplicity) that $F = I$.
- At last, “ $|f(x)| = 1$ a.e. sur Ω ”, is the binarity constraint. We have mentioned that the image f_o takes its values in $\{0, \lambda\}$ where $\lambda > 0$. With the change of variable $f = -\frac{2}{\lambda}f_o + 1$, we may assume that the image values belong to $\{-1, 1\}$.

Remark 3.4. *A similar problem has been studied in [4] with smoother projection operator and convex constraints. This is not our case. The pointwise constraint “ $|f(x)| = 1$ a.e. on Ω ” is a very hard constraint. The constraint set is not convex and its interior is empty for most usual topologies.*

Now we may give the main result of this section :

Theorem 3.1. *Problem (\mathcal{P}) admits at least a solution.*

Proof - Let $\varphi_n \in BV(\Omega)$ be a minimizing sequence. It satisfies $\|\varphi_n\|_\infty = 1$; so

$$\forall p \in [1, +\infty[, \forall n \in \mathbb{N}, \quad \|\varphi_n\|_{L^p} \leq |\Omega|^{\frac{1}{p}}. \quad (3.8)$$

Therefore the sequence (φ_n) is $L^1(\Omega)$ - bounded. As $J(\varphi_n)$ is bounded as well, the sequence is bounded in $BV(\Omega)$. Thus it converges (extracting a subsequence) to some $\varphi \in BV(\Omega)$ for the weak-star topology.

Estimate (3.8) implies the weak convergence of (φ_n) to φ in $L^{2+s}(\Omega)$ for every $s > 0$. Thanks to the H continuity property of proposition 3.4, we assert that $H\varphi_n$ weakly converges to $H\varphi$ in $L^2(\Omega)$. We get

$$\|H\varphi - g\|_{L^2}^2 \leq \liminf_{n \rightarrow \infty} \|H\varphi_n - g\|_{L^2}^2, \quad (3.9)$$

with the lower semi-continuity of the norm.

Moreover $BV(\Omega)$ is compactly embedded in $L^1(\Omega)$. This yields that (φ_n) strongly converges to φ in $L^1(\Omega)$. As J is lsc with respect to $L^1(\Omega)$ - topology, we get

$$J(\varphi) \leq \liminf_{n \rightarrow \infty} J(\varphi_n), \quad (3.10)$$

Finally

$$\begin{aligned} \inf(\mathcal{P}) &= \lim_{n \rightarrow +\infty} \|H\varphi_n - g\|_{L^2}^2 + \alpha J(\varphi_n) \\ &\geq \liminf_{n \rightarrow \infty} \|H\varphi_n - g\|_{L^2}^2 + \alpha J(\varphi_n) \geq \|H\varphi - g\|_{L^2}^2 + \alpha J(\varphi). \end{aligned}$$

As the pointwise constraint is obviously satisfied, φ is a solution to (\mathcal{P}) . \square

4. COMPUTATION OF THE ENERGY DERIVATIVE

Now we look for optimality conditions. Unfortunately we cannot compute easily the derivative of the energy in the $BV(\Omega)$ framework. Indeed we need regular curves and we do not know if the $BV(\Omega)$ minimizer provides a curve with the required regularity. Moreover, the set of constraints is not convex and it is not easy to compute the Gâteaux- derivative (no admissible test functions).

So we have few hope to get classical optimality conditions and we rather compute minimizing sequences. We focus on particular ones that are given via the gradient descent method inspired by [11]. Formally, we look for a family of curves $(\gamma_t)_{t \geq 0}$ such that

$$\frac{\partial E}{\partial \gamma}(\gamma_t) \leq 0$$

so that $E(\gamma_t)$ decreases as $t \rightarrow +\infty$. Let us compute the energy variation when we operate a small deformation on the curves γ . In other word, we will compute the Gâteaux derivative of the energy for a small deformation $\delta\gamma$:

$$\frac{\partial E}{\partial \gamma}(\gamma) \cdot \delta\gamma = \lim_{t \rightarrow 0} \frac{E(\gamma + t\delta\gamma) - E(\gamma)}{t}.$$

We will first focus on local deformations $\delta\gamma$. Let (r_0, z_0) be a point P of γ . We consider a local reference system which center is P and axis are given by the tangent and normal vectors at P and we denote by (ξ, η) the new generic coordinates in this reference system. With an abuse of notation, we still denote $f(\xi, \eta) = f(r, z)$. We apply the implicit functions theorem to parametrize our curve: there exist a neighborhood U of P and a \mathcal{C}^1 function h such that, for every $(\xi, \eta) \in U$,

$$(\xi, \eta) \in \gamma \iff \eta = h(\xi).$$

Eventually, we get a neighborhood U of P , a neighborhood I of ξ_0 and a \mathcal{C}^1 function h such that

$$\gamma \cap U = \left\{ (\xi, \eta) \in \mathbb{R}^2 \mid \eta = h(\xi), \xi \in I \right\}.$$

The local parametrization is oriented along the outward normal \vec{n} to the curve γ at point P (see figure 6). More precisely, we define the local coordinate system $(\vec{\tau}, \vec{n})$ where $\vec{\tau}$ is the usual tangent vector, \vec{n} is the direct orthonormal vector; we set the curve orientation so that \vec{n} is the outward normal. The function f is then defined on U by

$$f(\xi, \eta) = \begin{cases} \lambda & \text{if } \eta < h(\xi) \\ 0 & \text{if } \eta \geq h(\xi) \end{cases}$$

This parametrization is described on figure 6. We then consider a local (limited to U) deformation $\delta\gamma$ along the normal vector. This is equivalent to handling a \mathcal{C}^1 function δh whose support is

included in I . The new curve γ_t obtained after the deformation $t\delta\gamma$ is then parametrized by

$$\eta = \begin{cases} h(\xi) + t\delta h(\xi) & \text{for } (\xi, \eta) \in U \\ \gamma & \text{otherwise} \end{cases}$$

This defines a new function f_t :

$$f_t(\xi, \eta) = \begin{cases} f(\xi, \eta) & \text{if } (\xi, \eta) \notin U \\ \lambda & \text{if } (\xi, \eta) \in U \cap \{\eta < h(\xi) + t\delta h(\xi)\} \\ 0 & \text{if } (\xi, \eta) \in U \cap \{\eta \geq h(\xi) + t\delta h(\xi)\} \end{cases} \quad (4.11)$$

We will also set $\delta f_t = f_t - f$. This deformation is described on figure 6.

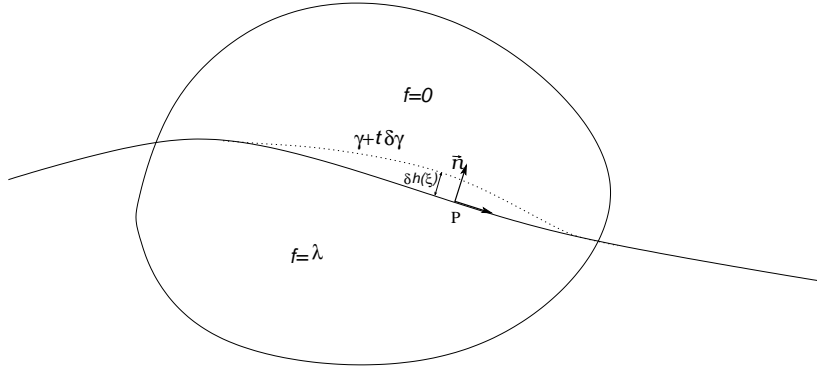


FIGURE 6. Description of a local deformation of the initial curve γ . P is the current point, U is the neighborhood of P in which the deformation is restricted to and $\gamma + t\delta\gamma$ is the new curve after deformation. The interior of the curve is the set where $f = \lambda$

The Gâteaux derivative for the energy E_2 has already been computed in [11] and is

$$\frac{\partial E_2}{\partial \gamma}(\gamma)\delta\gamma = - \int_{\gamma} \text{curv}(\gamma)(\xi, h(\xi))\delta h(\xi)d\xi$$

where curv denotes the curvature of the curve and δh is the parametrization of $\delta\gamma$.

It remains to compute the derivative for the matching term. First we estimate δf_t : a simple computation shows that

$$\delta f_t(\xi, \eta) = \begin{cases} 0 & \text{if } \eta \geq h(\xi) + t\delta h(\xi) \text{ or } \eta(\xi) \leq h(\xi) \\ \lambda & \text{if } h(\xi) \leq \eta \leq h(\xi) + t\delta h(\xi) \end{cases} \quad \text{in case } \delta h \geq 0$$

and

$$\delta f_t(\xi, \eta) = \begin{cases} 0 & \text{if } \eta \leq h(\xi) + t\delta h(\xi) \text{ or } \eta(\xi) \geq h(\xi) \\ -\lambda & \text{if } h(\xi) \geq \eta \geq h(\xi) + t\delta h(\xi) \end{cases} \quad \text{in case } \delta h \leq 0$$

Now we compute $E_1(\gamma_t) - E_1(\gamma)$ where γ (resp. γ_t) is the curve associated to the function f (resp. f_t):

$$\begin{aligned}
E_1(\gamma_t) - E_1(\gamma) &= \int_{\mathbb{R}} \int_{\mathbb{R}} ((g - FHf_t)^2 - (g - FHf)^2)(u, v) du dv \\
&= \int_{\mathbb{R}} \int_{\mathbb{R}} ((g - FHf - FH\delta f_t)^2 - (g - FHf)^2)(u, v) du dv \\
&= -2 \int_{\mathbb{R}} \int_{\mathbb{R}} (g - FHf)(u, v) FH\delta f_t(u, v) du dv + \underbrace{\int_{\mathbb{R}} \int_{\mathbb{R}} (FH\delta f_t)^2(u, v) du dv}_{=o(t)} \\
&= -2 \langle (g - FHf), FH\delta f_t \rangle_{L^2} + o(t) \\
&= -2 \langle H^*F^*(g - FHf), \delta f_t \rangle_{L^2} + o(t).
\end{aligned}$$

To simplify the notations, we denote by $\mathcal{A}f := (H^*F^*g - H^*F^*FHf)$ so that we need to compute

$$\lim_{t \rightarrow 0} \frac{1}{t} \langle \mathcal{A}f, \delta f_t \rangle_{L^2}.$$

As δf_t is zero out of the neighbourhood U , we have

$$\langle \mathcal{A}f, \delta f_t \rangle_{L^2} = \int_U \mathcal{A}f(\xi, \eta) \delta f_t(\xi, \eta) d\xi d\eta.$$

In the case $\delta h \geq 0$, we have,

$$\langle \mathcal{A}f, \delta f_t \rangle_{L^2} = \lambda \int_{\xi \in I} \int_{\eta=h(\xi)}^{\eta=h(\xi)+t\delta h(\xi)} \mathcal{A}f(\xi, \eta) d\xi d\eta.$$

As the function $\mathcal{A}f$ is continuous (and thus bounded on U), we may pass to the limit by dominated convergence and get

$$\lim_{t \rightarrow 0} \frac{1}{t} \langle \mathcal{A}f, \delta f_t \rangle_{L^2} = \lambda \int_I \mathcal{A}f(\xi, h(\xi)) \delta h(\xi) d\xi.$$

In the case $\delta h < 0$, we have

$$\langle \mathcal{A}f, \delta f_t \rangle_{L^2} = \int (-\lambda) \int_{\xi \in I} \int_{\eta=h(\xi)+t\delta h(\xi)}^{\eta=h(\xi)} \mathcal{A}f(\xi, \eta) d\xi d\eta$$

and we obtain the same limit as in the nonnegative case.

Finally, the energy derivative is

$$\frac{\partial E}{\partial \gamma}(\gamma_f) \cdot \delta \gamma_f = -2\lambda \int_I \mathcal{A}f(\xi, h(\xi)) \delta h(\xi) d\xi - \alpha \int_I \text{curv}(\gamma_f)(\xi, h(\xi)) \delta h(\xi) d\xi$$

If we set $\beta = \frac{\alpha}{2}$, we get

$$\frac{\partial E}{\partial \gamma}(\gamma_f) \cdot \delta \gamma_f = -2 \int_I (\lambda \mathcal{A}f + \beta \text{curv}(\gamma_f)(\xi, h(\xi))) \delta h(\xi) d\xi. \quad (4.12)$$

As $\delta h = \langle \delta \gamma_f, \vec{n} \rangle$ formula (4.12) may be written

$$\frac{\partial E}{\partial \gamma}(\gamma_f) \cdot \delta \gamma_f = -2 \int_{\gamma} (\lambda \mathcal{A}f + \beta \text{curv}(\gamma_f)(s)) \langle \delta \gamma_f, \vec{n} \rangle ds \quad (4.13)$$

where \vec{n} denotes the outward pointing normal unit vector of the curve γ , $\langle \cdot, \cdot \rangle$ denotes the usual scalar product in \mathbb{R}^2 and $c(s)$ is a positive coefficient that depends on the curvilinear abscissa s .

The latter expression is linear and continuous in $\delta \gamma$, this formula is also true for a non-local deformation (which can be achieved by summing local deformations).

5. FRONT PROPAGATION AND LEVEL SET METHOD

The goal of the present section is to consider a family of curves $(\gamma_t)_{t \geq 0}$ that will converge toward a local minimum of the functional energy. From equation (4.13), it is clear that if the curves (γ_t) evolve according to the differential equation

$$\frac{\partial \gamma}{\partial t} = (\lambda \mathcal{A}f + \beta \text{curv}(\gamma_f)) \vec{n}, \quad (5.14)$$

the total energy will decrease.

To implement a numerical scheme that discretizes equation (5.14), it is easier to use a level set method (see [12] for a complete exposition of the level set method). Indeed, equation (5.14) may present some instabilities, in particular when two curves collide during the evolution or when a curve must disappear. All these evolutions are handled easily via the level set method.

The level set method consists in viewing the curves γ as the 0-level set of a smooth real function ϕ defined on \mathbb{R}^2 . The function f that we are seeking is then just given by the formula

$$f(x) = \lambda \mathbf{1}_{\phi(x) > 0}.$$

We must then write an evolution PDE for the functions $\phi_t = \phi(t, \cdot)$ that corresponds to the curves γ_t . Let $x(t)$ be a point of the curve γ_t and let us follow that point during the evolution. We know that this point evolves according to equation 5.14

$$x'(t) = (\lambda \mathcal{A}f + \beta \text{curv}(\gamma_f))(x(t)) \vec{n}.$$

We can re-write this equation in terms of the function ϕ recognizing that

$$\vec{n} = \frac{\nabla \phi}{|\nabla \phi|} \quad \text{and} \quad \text{curv}(\gamma) = \text{div} \left(\frac{\nabla \phi}{|\nabla \phi|} \right)$$

where ∇ stands for the gradient of ϕ with respect to x , $|\cdot|$ denotes the euclidean norm. The evolution equation becomes

$$x'(t) = \left(\lambda \mathcal{A} (\lambda 1_{\phi(t,\cdot) > 0}) + \beta \operatorname{div} \left(\frac{\nabla \phi}{|\nabla \phi|} \right) \right) \frac{\nabla \phi}{|\nabla \phi|}(t, x(t)).$$

Then, as the point $x(t)$ remains on the curve γ_t , it satisfies $\phi_t(x(t)) = \phi(t, x(t)) = 0$. By differentiating this expression, we obtain

$$\frac{\partial \phi}{\partial t} + \langle \nabla \phi, x'(t) \rangle = 0$$

which leads to the following evolution equation for ϕ :

$$\frac{\partial \phi}{\partial t} + |\nabla_x \phi| \left(\lambda \mathcal{A} (\lambda 1_{\phi(t,\cdot) > 0}) + \beta \operatorname{div} \left(\frac{\nabla \phi}{|\nabla \phi|} \right) \right) = 0,$$

that is

$$\frac{\partial \phi}{\partial t} = |\nabla \phi| \left(\lambda^2 H^* F^* F H (1_{\phi(t,\cdot) > 0}) - \beta \operatorname{div} \left(\frac{\nabla \phi}{|\nabla \phi|} \right) - \lambda H^* F^* g \right). \quad (5.15)$$

The above equation is an Hamilton-Jacobi equation which involves a non local term (through H and F). Such equations are difficult to handle especially when it is not monotone (which is the case here). In particular, existence and/or uniqueness of solutions (even in the viscosity sense) are not clear. The approximation process is not easy as well and the numerical realization remains a challenge though this equation is a scalar equation which is easier to discretize than the vectorial one. Here we used the discrete scheme described in [12] to get numerical results.

6. RESULTS AND DISCUSSION

6.1. Explicit scheme

We briefly present the numerical scheme. We used an explicit scheme in time and the spatial discretization has been performed following [12]. We set

$$\mathcal{G} = (FH)^* FH \text{ and } g^* = H^* F^* g,$$

so that the equation (5.15) is

$$\frac{\partial \phi}{\partial t} = |\nabla \phi| \left(\lambda^2 \mathcal{G} (1_{\phi(t,\cdot) > 0}) - \beta \operatorname{div} \left(\frac{\nabla \phi}{|\nabla \phi|} \right) - \lambda g^* \right).$$

We set $t_n = n\Delta t$, $\Phi^n = \phi(t_n, \cdot)$, $X = (x_i, y_j)_{(i,j) \in I}$ with $x_i = i\Delta x$ et $y_j = j\Delta y$. The explicit Euler scheme gives :

$$\Phi^{n+1}(X) = \Phi^n(X) + \Delta t |\nabla \Phi^n|(X) \left(\lambda^2 \mathcal{G}(1_{\Phi^n > 0}) - \beta \operatorname{curv}(\Phi^n) - \lambda g^*(t_n, X) \right).$$

The curvature term is computed as

$$\text{curv}(\Phi) = \frac{\Phi_{xx}(\Phi_y)^2 - 2\Phi_x\Phi_y\Phi_{xy} + \Phi_{yy}(\Phi_x)^2}{((\Phi_x^2 + \Phi_y^2)^{3/2}},$$

where Φ_x stands for the partial derivative with respect to x . The discrete approximation of the gradient is standard:

$$D_x^+\Phi(x, y) = \frac{\Phi(x + \Delta x, y) - \Phi(x, y)}{\Delta x}, \quad D_x^-\Phi(x, y) = \frac{\Phi(x, y) - \Phi(x - \Delta x, y)}{\Delta x};$$

$D_y^+\Phi$ and $D_y^-\Phi$ defined in the same way. A usual approximation for $|\nabla\Phi|$ is given by :

$$|\nabla\Phi|(X) \simeq [\max(D_x^+\Phi, 0)^2 + \max(D_y^+\Phi, 0)^2 + \min(D_x^-\Phi, 0)^2 + \min(D_y^-\Phi, 0)^2]^{1/2}.$$

The non local term $\mathcal{G}(1_{\Phi^n > 0})$ is exactly computed.

6.2. Numerical results

The previous scheme has been implemented on a 3.6 GHz PC. A classical reinitialization process has been used each 500 iterations. The test image size was 256×256 pixels. The other parameters of the computation were set to

$$\alpha = 10, \quad \lambda = 2, \quad \Delta x = 1 \quad \text{and} \quad \Delta t = 10^{-4}$$

and the blur kernel is a Gaussian kernel of standard deviation 5 pixels.

The computed image is quite satisfying (see figure 7.) However, we note a bad reconstruction along the symmetry axis due to the problem geometry and a lack of information. Moreover we have to improve the algorithm behavior. Indeed, we observe numerical instability (in spite of the regularization process) that leads to a very small time step choice. Therefore the computational time is quite long (about 2.5 hours). In addition, classical stopping criteria are not useful here : the expected solution corresponds to a “flat” level of function Φ and the difference between two consecutive iterates means no sense. An estimate of the cost function decrease is not appropriate as well (we observe oscillations). We decided to stop after a large enough number of iterations (here 20 000).

In spite of all these disadvantages, this method is satisfactory considering the low signal to noise ratio of the radiograph. These good results can be explained by the strong assumptions that we add (in particular the binary hypothesis) which are verified by our synthetic object. Anyway, the method has been successfully tested on “real” images as well, that is images of objects with the same kind of properties (“almost” binary) but we cannot report them here (confidential data). A semi-implicit version of the algorithm is actually tested to improve stability.



FIGURE 7. Experimental results

REFERENCES

- [1] **I. Abraham, R. Abraham** Technical Report CEA (2001).
- [2] **L. Ambrosio, N. Fusco et D. Pallara**, *Functions of bounded variation and free discontinuity problems*, Oxford mathematical monographs, Oxford University Press, 2000.
- [3] **J.P. Bruandet, F. Peyrin, J.M. Dinten, M. Barlaud** *3D tomographic reconstruction of binary images from cone-beam projections: a fast level-set approach*
2002 IEEE International Symposium on Biomedical Imaging, p. 677-80, (2002)
- [4] **E. Casas, K. Kunisch and C. Pola**, *Regularization by Functions of Bounded Variation and Applications to Image Enhancement*, Applied Mathematics and Optimization, 40:229257 (1999)
- [5] **J.-M. Dinten** *Tomographie à partir d'un nombre limité de projections : régularisation par champs markovien*
PHD thesis, Université d'Orsay Paris-Sud (1990)
- [6] **N. J. Dusaussoy** *Image reconstruction from projections*
SPIE's international symposium on optics, imaging and instrumentation. San Diego (1994)
- [7] **H. Feng, W. Karl, D. Castanon** *A curve evolution approach to object-based tomographic reconstruction*
IEEE Trans. on Image Proc., 12, 44-57, (2003)
- [8] **K. Hanson** *Tomographic reconstruction of axially symmetric objects from a single radiograph*
High Speed Photography, 491, (1984)
- [9] **G. Herman** *Image reconstruction from projections: the fundamentals of computerized tomography*
Academic Press (1980)
- [10] **J.M. Lagrange** *Reconstruction tomographique à partir d'un petit nombre de vues*
PHD thesis, ENS Cachan (1998)
- [11] **D. Mumford - J. Shah** *Optimal approximations by piecewise smooth functions and associated variational problem*
Comm. Pure and Appl. Math. 42, 577-685 (1989)
- [12] **J.A. Sethian** *Theory, algorithm and applications of level set method for propagating interfaces*
Iserles, A. (ed.), Acta Numerica Vol. 5, 1996. Cambridge: Cambridge University Press. 309-395 (1996)
- [13] **E. Stein** *Singular integrals and differentiability properties of functions*, Princeton University Press